

とした IFN 単独長期療法を考慮すべきである。

9. 天然型 IFN-β + ribavirin 併用療法

a ポイント

- うつ病・うつ状態など IFN-α が不適応および、PEG-IFN-α + ribavirin 併用療法でうつ状態が出現した症例に対しては天然型 IFN-β + ribavirin 併用療法を選択する。
- IFN-α 製剤に比し脱毛が少ない。
- IFN-α 製剤に比し概して投与中の QOL が良好であり、高齢者で比較的使用しやすい。

b 天然型 IFN-β + ribavirin 併用療法の実際

表 38

保険適用	高ウイルス量 (5 logIU/mL 以上) の C 型慢性肝炎におけるウイルス血症の改善
投与量の目安	<ul style="list-style-type: none"> ● 天然型 IFN-β (フェロン) は 1 日 600 万国単位で投与を開始し、投与後 4 週間までは連日、以後週 3 回静脈内投与または点滴静注する ● ribavirin (レベトール) の投与量は、ペグイントロン + レベトール併用療法と同じ
投与期間	24~48 週
開始基準	Hb 濃度が 12 g/dL 以上であることが望ましい
減量・中止基準	<ul style="list-style-type: none"> ● フェロンの減量基準は表 39 参照 ● Hb 濃度による ribavirin の減量基準は、ペグイントロン + レベトール併用療法と同じ
効果判定	ウイルス学的効果・生化学的効果を判定・治療中の抗ウイルス効果を判定
治療成績	表 40 参照

IV 章

肝炎・肝硬変の主な治療法

表 39 白血球数，好中級数，血小板数による薬剤の減量基準

検査項目	数 値	ribavirin	IFN-β
白血球数	1,500/μL 未満	用量変更なし	半量に減量
好中球数	750/μL 未満		
血小板数	50,000/μL 未満		
白血球数	1,000/μL 未満	中止	中止
好中球数	500/μL 未満		
血小板数	25,000/μL 未満		

c 治療成績

表 40 治療成績 (国内開発治験の成績：24 週投与のウイルス学的著効率)

患者群	IFN-β+ribavirin 群	IFN-α2b+ribavirin 群
セログループ 1 かつ高ウイルス量	18.7% (17/91)	15.6% (7/45)
セログループ 1 かつ高ウイルス量 または IFN 治療歴の ある低ウイルス量	75.0% (15/20)	83.3% (10/12)

10. PEG-IFN-α2a 単独療法

a ポイント

- PEG-IFN で単独投与が認められているのは、PEG-IFN-α2a (40kDa) である (表 41)。
- ゲノタイプ 2 の完遂例では 84% の高い著効率が得られている。
- ribavirin を併用しないため食欲不振、貧血などの副作用が少なく忍容性がよい。
- 副作用の種類は非修飾型 IFN と同じである。発熱、倦怠感、悪寒、不眠の頻度は非修飾型 IFN より低いですが、痒症、注射部位の発赤や血小板減少などの有害事象の頻度は高い。
- SVR が期待できない症例に対して、肝炎進行防止・肝発癌抑止を目的として行われることがある。

表 41 PEG-IFN-α2a 単独療法の適応

ウイルス駆除を目的とした治療
<ul style="list-style-type: none"> • ribavirin 使用不可例 • 低ウイルス量の初回治療例 • ゲノタイプ 1：中ウイルス症例 (著効率 33%) • ゲノタイプ 2 の症例 (完遂例の著効率 84%)
肝炎進行防止・肝発癌抑止を目的とした治療
<ul style="list-style-type: none"> • ribavirin 使用不可例 (高齢者、妊娠可能な若年層、貧血、心疾患、腎疾患合併例など) • PEG-IFN+ribavirin 併用療法で非著効となった症例

b PEG-IFN- α 2a 単独療法の実際

表 42

保険適用	C型慢性肝炎におけるウイルス血症の改善 すべてのゲノタイプとウイルス量に適応がある
投与量の目安	PEG-IFN- α 2a (ペガシス)：180 μ g の固定用量
投与期間	24～48 週 (ただし、投与期間の制限はない)
開始基準	表 43 参照 (ribavirin 併用療法と異なる)
減量・中止基準	表 44 参照. 毎回投与直前に必ず血液検査を実施し この基準を満たしているか確認してから投与する (ribavirin 併用療法と異なる)
効果判定	ウイルス学的効果・生化学的効果を判定・治療中の 抗ウイルス効果を判定
治療成績	表 46 参照

表 43 開始基準

検査項目	投与前値
好中球数	1,500/ μ L 以上
血小板数	90,000/ μ L 以上
Hb 量	10 g/ μ L 以上

表 44 減量・中止基準

検査項目	90 μ g に減量	中止
好中球数	750/ μ L 未満	500/ μ L 未満
血小板数	50,000/ μ L 未満	25,000/ μ L 未満
Hb 量	—	8.5 g/ μ L 未満

c PEG-IFN- α 2a 単独療法の禁忌

表 45

- ◆ 小柴胡湯を投与中の患者
- ◆ AIH の患者
- ◆ IFN に対し過敏症のある患者
- ◆ 3 歳未満
- ◆ 生物学的製剤に対し過敏症のある患者

d 治療成績 (国内開発治験におけるウイルス学的著効率)

表 46

ゲノタイプ	ウイルス量	180 μ g/週投与群	90 μ g/週投与群
1b	100 kIU/mL 以上	16%	13%
	100 kIU/mL 未満	57%	50%
2a, 2b	100 kIU/mL 以上	76%	27%
	100 kIU/mL 未満	62%	86%
合 計		36%	27%

11. IFN 単独療法 (自己注射も含む)

- ribavirin 禁忌例や HCV RNA < 5 logIU/mL の低ウイルス量例に推奨される。65 歳以上の高齢者や貧血、腎障害、糖尿病および高血圧などの合併例では、本療法も選択肢となる。
- IFN 製剤間の抗ウイルス効果には大きな差はない。
- 難治例でも長期療法 (>2 年) により SVR や SBR が得られることがある。
- IFN 単独療法に投与期間の制限は撤廃されている。
- SVR が達成できない症例に対し、肝機能の正常化と肝発癌抑止を目的として行われることが多い。
- 自己注射が 2 週間に 1 度の受診を条件に可能となった。自己注射専用の製剤があるのは、天然型 IFN- α (スミフェロン) である。
- 自己注射のメリットとして、夜間投与があげられる。夜間投与により、発熱、倦怠感などの副作用を軽減できる。
- IFN 単独療法では、IFN- β を使用することができる。
- IFN- β は、 α 製剤に比し精神・神経系の副作用がより少ないため、高齢者や精神疾患の既往がある患者には比較的投与しやすい。

a IFN- β の特徴

- 天然型製剤で静注または点滴静注で投与する。
- 肝硬変にも保険適用がある (フェロン)。
- 肝硬変に対する適応は、ゲノタイプ 1 かつ高ウイルス量以

外の症例である。

- 精神・神経系の副作用が α 製剤より少ないため、高齢者や精神疾患の既往がある患者には比較的投与しやすい。
- α 製剤に比し脱毛が少ない。
- 概して投与中のQOLが α 製剤より良好である。
- 蛋白尿の出現頻度が高い。

12. C型肝硬変に対するIFN療法

- C型肝硬変に対しても天然型IFN- α （スミフェロン）単独，天然型IFN- β （フェロン）単独，PEG-IFN- α 2a+ribavirin併用療法およびPEG-IFN- α 2b+ribavirin併用療法が保険適用となっている。
- IFNは代償性肝硬変に有用である。慢性肝炎より著効率が低く，副作用発生率，脱落率が高いが，著効が得られれば予後が改善する。
- 薬剤投与量や減量中止基準はC型慢性肝炎に対するものと異なるので注意が必要である。

a C型代償性肝硬変に対する天然型IFN- α 単独療法

表 47 天然型IFN- α 投与の実際

保険適用	● C型代償性肝硬変におけるウイルス血症の改善（セログループ1の血中HCV RNA量が高い場合を除く）
投与量の目安	天然型IFN- α （スミフェロン）を1日1回600万国単位で投与を開始し，投与後2週間までは連日，その後1日1回300万～600万国単位を週3回皮下または筋肉内に投与する
減量・中止基準	<ol style="list-style-type: none"> 1. 白血球数1,500/μL未満，血小板数30,000/μL未満，ALT（GPT）値500IU/L以上などの著しい異常が認められた場合には投与を中止し，適切な処置を行う 2. 血小板数30,000/μL以上50,000/μL未満などの異常が認められた場合には減量または投与間隔を延長する 3. 血算は投与開始後2週間の連日投与期間は少なくとも2～4日に1回，以後連日投与終了2週間後に1回，その後は4週間ごとに1回を目安として実施し，投与開始から2週間は入院により管理することが望ましい
効果判定	表 14 参照

表 48 C型代償性肝硬変に対する天然型 IFN- α の治療成績 (国内開発治験)

セログループ	HCV RNA 量* (KIU/mL)	HCV RNA 陰性化率		ALT (GPT) 正常化率		AST (GOT) 正常化率	
		投与終了24週後	投与終了時	投与終了24週後	投与終了時	投与終了24週後	投与終了時
1	100 未満	80.0% (4/5)	33.3% (1/3)	66.7% (2/3)	50.0% (2/4)	75.0% (3/4)	
	100 以上 500 未満	22.2% (4/18)	23.1% (3/13)	15.4% (2/13)	27.8% (5/18)	11.1% (2/18)	
	500 以上	0.0% (0/9)	66.7% (4/6)	0.0% (0/6)	42.9% (3/7)	0.0% (0/7)	
2	100 未満	68.8% (11/16)	81.8% (9/11)	72.7% (8/11)	63.6% (7/11)	63.6% (7/11)	
	100 以上 500 未満	20.8% (5/24)	45.0% (9/20)	35.0% (7/20)	41.7% (10/24)	33.3% (8/24)	
	500 以上	5.9% (1/17)	69.2% (9/13)	38.5% (5/13)	57.1% (8/14)	28.6% (4/14)	

*アンプリコアモニター法により測定 (投与開始前)。

b C型代償性肝硬変に対する天然型 IFN- β 単独療法

表 49 天然型 IFN- β 投与の実際

保険適用	●C型代償性肝硬変におけるウイルス血症の改善 (ゲノタイプ1かつ高ウイルス量以外)
投与量の目安	天然型 IFN- β (フェロン) : 300~600万単位/日, 静注または点滴静注
減量・中止基準	表 50 参照
治療成績	表 51 参照

表 50 IFN- β 減量・中止基準

検査項目	減量または投与間隔の延長	中止
白血球数	1,500/ μ L 未満	1,000/ μ L 未満
好中球数	750/ μ L 未満	500/ μ L 未満
血小板数	50,000/ μ L 未満	25,000/ μ L 未満

表 51 C型代償性肝硬変に対する天然型 IFN- β の治療成績*

投与期間	ウイルス学的著効率	生化学的著効率
6~7週	15%	17%
20~22週	29%	29%
34~36週	39%	41%

*対象はゲノタイプ 1b かつ高ウイルス量以外.

C C型代償性肝硬変に対する PEG-IFN- α 2a+ribavirin 併用療法

表 52 PEG-IFN- α 2a+ribavirin 併用療法の実際

保険適用	● C型代償性肝硬変におけるウイルス血症の改善
投与量の目安	● PEG-IFN- α 2a(ペガシス)の投与量は 90 μ g/週 ● ribavirin (コペガス) 投与量は C型慢性肝炎と同様
開始・減量・中止基準	表 53, 54 参照
治療成績	表 55 参照

表 53 開始基準

検査項目	投与前値
白血球数	3,000/ μ L 以上
好中球数	1,500/ μ L 以上
血小板数	75,000/ μ L 以上
Hb 量	12 g/dL 以上

表 54 減量・中止基準

検査項目	数 値	ribavirin	PEG-IFN- α 2a (遺伝子組換え)
好中球数	1,000/ μ L 未満	変更なし	45 μ g に減量
	750/ μ L 未満	変更なし	22.5 μ g に減量
	500/ μ L 未満	中止	中止
血小板数	50,000/ μ L 未満	中止	中止 (50,000/ μ L 以上に回復後 45 μ g で再開可)
	35,000/ μ L 未満	中止	中止 (50,000/ μ L 以上に回復後 22.5 μ g で再開可)
	25,000/ μ L 未満	中止 (再開不可)	中止 (再開不可)
Hb 量 (心疾患 またはそ の既往な し)	投与開始 1~4 週時 11 g/dL 未 満	減量 600 mg/日 \rightarrow 200 mg/日 800 mg/日 \rightarrow 400 mg/日 1,000 mg/日 \rightarrow 400 mg/日	変更なし
	投与開始 5~ 48 週時 10 g/dL 未満	減量 600 mg/日 \rightarrow 200 mg/日 800 mg/日 \rightarrow 400 mg/日 1,000 mg/日 \rightarrow 400 mg/日	変更なし
	8.5 g/dL 未満	中止	中止
Hb 量 (心疾患 またはそ の既往あ り)	投与開始 1~4 週時 11 g/dL 未 満, または投与 中, 投与前値に 比べ 2 g/dL 以 上の減少が 4 週間持続	減量 600 mg/日 \rightarrow 200 mg/日 800 mg/日 \rightarrow 400 mg/日 1,000 mg/日 \rightarrow 400 mg/日	変更なし
	投与開始 5~ 48 週時 10 g/dL 未満, または投 与中, 投与前 値に比べ 2 g/ dL 以上の減少 が 4 週間持続	減量 600 mg/日 \rightarrow 200 mg/日 800 mg/日 \rightarrow 400 mg/日 1,000 mg/日 \rightarrow 400 mg/日	変更なし
	8.5 g/dL 未満, または減量後, 4 週間経過して も 12 g/dL 未満	中止	中止

表 55 C型代償性肝硬変に対するPEG-IFN- α 2a+ribavirinの治療成績（国内開発治験の成績）

ゲノタイプ	ウイルス量	90 μ g 群
1a, 1b	≥ 100 KIU/mL	8/45 (17.8%)
1a, 1b	≥ 500 KIU/mL	6/40 (15.0%)
1a, 1b	100~500 KIU/mL	2/5 (40.0%)
1a, 1b	<100 KIU/mL	2/3 (66.7%)
1a, 1b	合計	10/48 (20.8%)
2a, 2b	≥ 100 KIU/mL	5/11 (45.5%)
2a, 2b	≥ 500 KIU/mL	1/6 (16.7%)
2a, 2b	100~500 KIU/mL	4/5 (80.0%)
2a, 2b	<100 KIU/mL	1/1 (100%)
2a, 2b	合計	6/12 (50.0%)
不明	≥ 500 KIU/mL	1/1 (100%)
合計	合計	17/61 (27.9%)

d C型代償性肝硬変に対するPEG-IFN- α 2b+ribavirin併用療法

表 56 PEG-IFN- α 2b+ribavirin併用療法の実際

保険適用	<ul style="list-style-type: none"> C型代償性肝硬変におけるウイルス血症の改善
投与量の目安	<ul style="list-style-type: none"> PEG-IFN-α2b（ペグイントロン）の投与量は1.0μg/kg/週 ribavirin（レベトール）投与量は体重別であるが、Hb濃度により異なる（表57参照）
開始・減量・中止基準	表58, 59参照
治療成績	表60参照

表 57 ribavirin（レベトール）の投与量

投与開始前のHb濃度	体 重	ribavirinの投与量		
		1日投与量(mg)	朝食後(mg)	夕食後(mg)
14 g/dL 以上	60 kg 以下	600	200	400
	60 kg を超え 80 kg 以下	800	400	400
	80 kg を超える	1,000	400	600
14 g/dL 未満	60 kg 以下	400	200	200
	60 kg を超え 80 kg 以下	600	200	400
	80 kg を超える	800	400	400

■表 58 開始基準

検査項目	投与前値
好中球数	1,500/ μ L 以上
血小板数	70,000/ μ L 以上
Hb 濃度	12 g/dL 以上

■表 59 減量・中止基準

検査項目	数 値	ribavirin	本 剤
好中球数	750/ μ L 未満	変更なし	半量に減量
	500/ μ L	中止	
血小板数	50,000/ μ L 未満	変更なし	半量に減量
	35,000/ μ L 未満	中止	
Hb 濃度 (投与開始 前の Hb 濃 度が 14 g/ dL 以上)	10 g/dL 未満	減量 400 mg/日 \rightarrow 400 mg/日 800 mg/日 \rightarrow 600 mg/日 1,000 mg/日 \rightarrow 600 mg/日	変更なし
	8.5 g/dL 未満	中止	
Hb 濃度 (投与開始 前の Hb 濃 度が 14 g/ dL 未満)	10 g/dL 未満	減量 400 mg/日 \rightarrow 200 mg/日 600 mg/日 \rightarrow 400 mg/日 800 mg/日 \rightarrow 400 mg/日	変更なし
	8.5 g/dL 未満	中止	

■表 60 C 型代償性肝硬変に対する PEG-IFN- α 2b+ribavirin の 48 週投与における治療成績

	ウイルス血症改善度
ゲノタイプ 1 かつ高ウイルス量	21.7% (15/69)
「ゲノタイプ 1 かつ高ウイルス量」以外	78.8% (26/33)
全 体	40.2% (41/102)

- 心疾患またはその既往がある患者に投与する場合には、Hb 濃度が 10 g/dL 以上であっても投与前に比べ 2 g/dL 以上の減少が 4 週間持続する場合は ribavirin の減量を、Hb 濃度が 8.5 g/dL 以上であっても減量後 4 週間経過しても 12 g/dL 未満の場合には投与中止を考慮する。

13. IFN 療法と C 型肝炎の予後

- IFN 著効例では、肝線維化、肝発癌、予後が改善する。非著効例でも予後が改善する可能性がある。
- 肝発癌率の減少：IFN 治療群は非治療群より有意に肝発癌が減少した。

14. 慢性肝炎以外への IFN 療法の適応拡大

- IFN の適用は急性肝炎、肝硬変、肝細胞癌の再発予防、ALT 正常の無症候性キャリアおよび HCV 関連肝外合併症である。
- 腎疾患：メサンギウム増殖性糸球体腎炎と膜性増殖性糸球体腎炎が多い。IFN で HCV RNA が低下すれば蛋白尿は改善するが、腎機能が改善することはまれである。治療終了後、再発する症例が多い。クレアチニンクリアランス低下例では ribavirin 併用療法は禁忌である。
- 血液疾患：有症状の本態性混合型クリオグロブリン血症は IFN 療法の適応である。

B

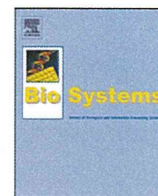
DAAs—C 型肝炎に対する新規治療薬

1. 作用機序

- HCV の増殖を直接抑える内服薬を総じて **direct-acting antiviral agents (DAAs)** 薬と呼称している。
- HCV は RNA ウイルスで図 3 のような構造になっている。
- ウイルス増殖に必要な酵素は主として非構造蛋白領域に存在し、主たる標的となっているのが NS3 のセリンプロテアーゼと NS5B に存在するポリメラーゼである。また、作用機序が明確になっていないが、NS5A はウイルス増殖や粒子形成あるいは IFN 感受性に重要な役割を担っているが、この部分が薬剤の重要な標的になっている (図 3)。
- 単独では効果が不十分なので併用治療が行われる。

IV 章

肝炎・肝硬変の主な治療法



Reproducibility and usability of chronic virus infection model using agent-based simulation; comparing with a mathematical model

Jun Itakura^{a,*}, Masayuki Kurosaki^a, Yoshie Itakura^a, Sinya Maekawa^b, Yasuhiro Asahina^a, Namiki Izumi^a, Nobuyuki Enomoto^b

^a Division of Gastroenterology and Hepatology, Musashino Red Cross Hospital, 1-26-1 Kyonan-cho, Musashino-shi, Tokyo 180-8610, Japan

^b First Department of Internal Medicine, Faculty of Medicine, University of Yamanashi, 1110, Shimogatou, Chuo-shi, Yamanashi 409-3898, Japan

ARTICLE INFO

Article history:

Received 30 June 2009

Received in revised form 27 August 2009

Accepted 6 September 2009

Keywords:

Agent-based model

Virus infectious disease

ABSTRACT

We created agent-based models that visually simulate conditions of chronic viral infections using two software. The results from two models were consistent, when they have same parameters during the actual simulation. The simulation results comprise a transient phase and an equilibrium phase, and unlike the mathematical model, virus count transit smoothly to the equilibrium phase without overshooting which correlates with actual biology in vivo of certain viruses. We investigated the effects caused by varying all the parameters included in concept; increasing virus lifespan, uninfected cell lifespan, uninfected cell regeneration rate, virus production count from infected cells, and infection rate had positive effects to the virus count during the equilibrium period, whereas increasing the latent period, the lifespan-shortening ratio for infected cells, and the cell cycle speed had negative effects. Virus count at the start did not influence the equilibrium conditions, but it influenced the infection development rate. The space size had no intrinsic effect on the equilibrium period, but virus count maximized when the virus moving speed was twice the space size. These agent-based simulation models reproducibly provide a visual representation of the disease, and enable a simulation that encompasses parameters those are difficult to account for in a mathematical model.

© 2009 Elsevier Ireland Ltd. All rights reserved.

1. Introduction

All viruses need hosts as a basis for their life. When a virus enters the host body, it invades cells and uses both its own enzymes and those of the host cells to replicate. Host cells infected by viruses launch a self-defense system known as the innate immune system (See and Wark, 2008; Nanche, 2009), which inhibits viral replication and uses the human leukocyte antigen system and cytokines to elicit an immune response. Immune cells that have received signals from host cells activate other immune cells, neutralize viruses in the serum by means of antibodies, and prevent the virus from replicating and proliferating by destroying or curing host cells. Viral infection is a disorder based on the interactions between viruses and cells.

The power relationship between these agents changes along with the progression of the disease. In the very early stages of infection, as the host defense mechanisms are immature, the virus has the ability to overwhelm the host cells, actively replicate, and proliferate. Subsequently, as the capacity of the immune system improves, the speed of viral proliferation drops and the virus count reaches a peak. Infected host cells begin to be disrupted by the immune system or virus particles, and symptoms appear as a result. If the immune system is stronger than the virus, then the viral counts decline, and, in transient viral disorders, the virus is finally eliminated and the host recovers. In chronic viral disorders, however, the power relationship between the virus and host cells reaches equilibrium, and a long-term power balance is maintained with the virus count reaching a plateau.

Mathematical models have been proposed to study the dynamics of such viral disorders, and are regarded as being of value in understanding this phenomenon (Ho et al., 1995; Nowak et al., 1996; Neumann et al., 1998). However, these models are difficult to understand for clinicians, and their applicability is somewhat limited in everyday practice. In clinical research, measurements of viral dynamics in patients for short duration have been made for human

Abbreviations: HIV, human immunodeficiency virus; HBV, hepatitis B virus; HCV, hepatitis C virus.

* Corresponding author. Tel.: +81 422 32 3111; fax: +81 422 32 9551.

E-mail address: jitakura@musashino.jrc.or.jp (J. Itakura).

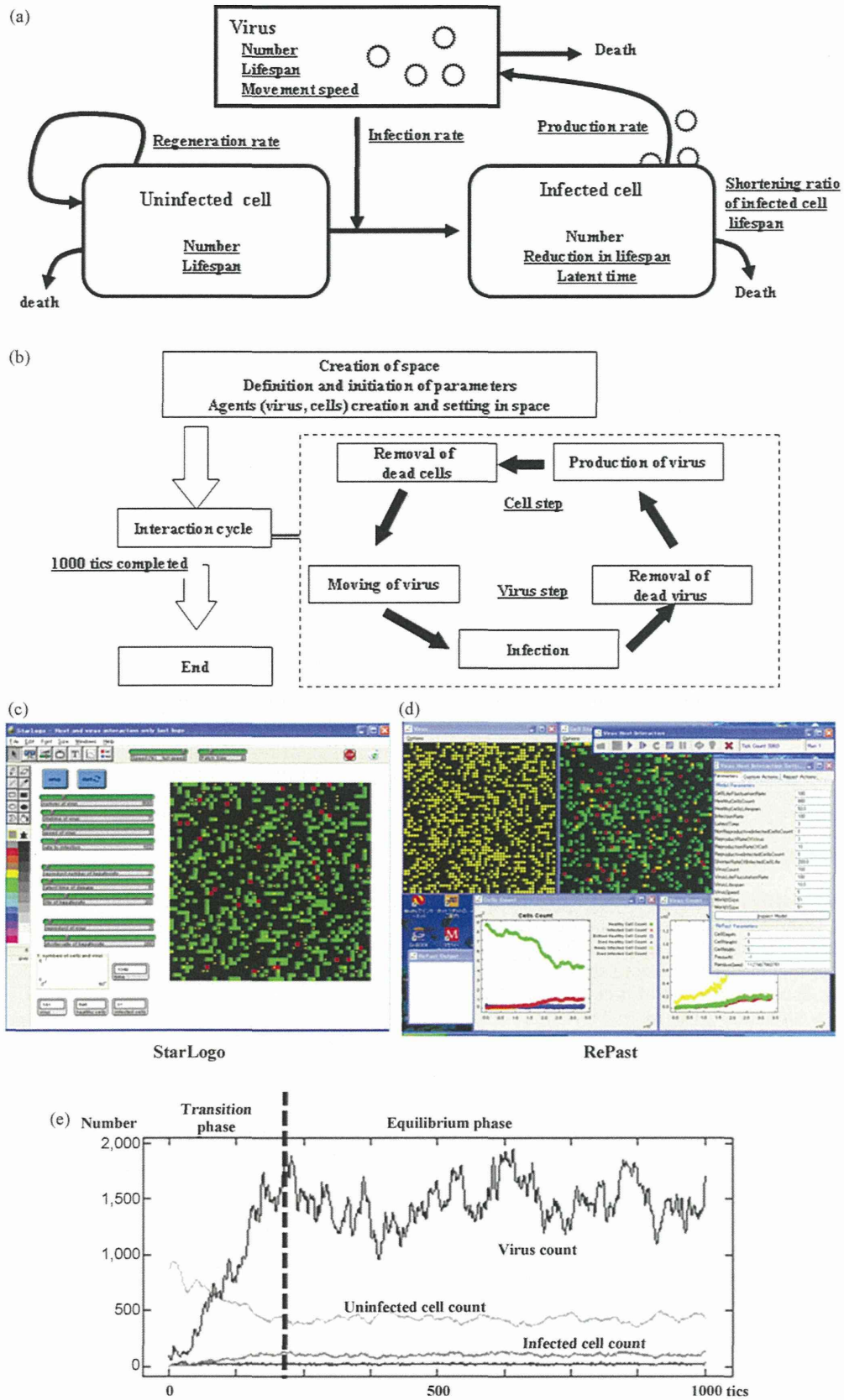


Fig. 1. Simulation design and an example of simulation results. (a) Model concept. Viruses, uninfected cells, and infected cells were treated as agents, and parameters were set for each of these and for interactions between agents (underlined). (b) Flowchart of the program. After preparing the simulation, we entered the interaction cycle, in which virus steps (such as movement) and cell steps were repeated. One cycle was counted as 1 tic, and the simulation concluded after 1000 tics. (c and d) Simulation screen using (c) StarLogo and (d) RePast. Yellow circles are viruses, green squares are uninfected cells, and orange and red indicate infected cells, with orange indicating the latent period. In StarLogo, all the agents are shown on the same screen, but in RePast, viruses and cells are shown in separate windows. (e) Example of a simulation chart in StarLogo. After the start of simulation the virus count and infected cell count increase while the uninfected cell count decreases, with equilibrium state reached after a certain number of tics.

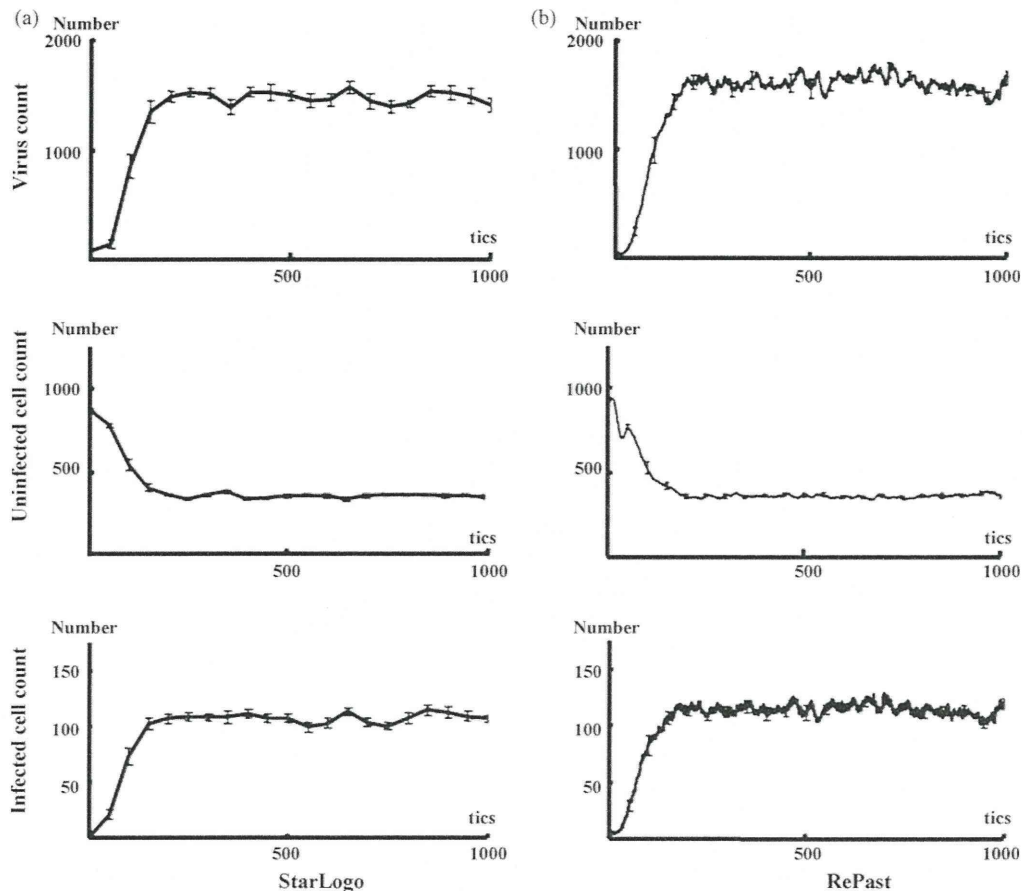


Fig. 2. Comparison of simulation results in (a) StarLogo and (b) RePast. The results were consistent when the parameters were made consistent. (Virus count [average \pm SD]: StarLogo 1458.03 ± 173.1 , RePast 1462.71 ± 178.8 , $p = 0.94$. Uninfected cell count: 364.24 ± 30.4 , 368.11 ± 33.4 , $p = 0.83$. Infected cell count: 105.73 ± 13.0 , 107.74 ± 13.0 , $p = 0.24$. Unpaired Student's *t*-test.) Parameter values were set as follows: initial virus count, 100; uninfected cell count, 880; infected cell count, 0; virus speed of movement, 5 grids/tic; infection rate, 10%; uninfected cell regeneration rate, 1%; latent period, 3 tics; and virus reproduction rate, 5/cells/tic. The following parameter settings were taken from actual measurements: virus lifespan, 4.5 tics; uninfected cell lifespan, 49.8 tics; and infected cell lifespan, 6.7 tics.

immunodeficiency virus (HIV) (Ho et al., 1995), hepatitis B virus (HBV) (Nowak et al., 1996) and hepatitis C virus (HCV) (Neumann et al., 1998), and research is also underway on a range of models based on animal experiments and cell culture systems. As chronic viral disorders persist over long periods of time complete follow-up of viral dynamics is difficult. Furthermore, limitations of items that can be measured, such as the difficulty of measuring whole numbers of host cells, make it extremely difficult to investigate their consistency in mathematical models.

The recent ascend of dynamic-models owes much to advances in computers. Computer performance has improved markedly in recent years, not only in terms of their calculating capacity but also with regard to image displays, and models that offer a visual representation of viral disorders are now being reported (Gilbert and Bankes, 2002; Duca et al., 2007; Shapiro et al., 2008; Castiglione et al., 2007). One advantage of such visual models is that by providing a visual representation, they make understanding the disease status easy. Another benefit is that they enable parameters to be identified that are hidden as background noise in mathematical models. However, these models have some problems; it is difficult to prove the reproducibility of the simulation results derived from different languages or libraries, difficult to prove the validity of the model's concepts, and difficult to prove that the simulation results accurately reflect the reality. In this study, we created agent-based computer models that visually simulate the conditions of chronic viral infections using two software. The reproducibility of two agent-based computer models and the differences between agent-based models and the mathematical model were analyzed.

This agent-based model enabled us to investigate how each parameter included in the concept affects the conditions of chronic viral infections.

2. Methods

2.1. Selection of Software

In this study, we used two different types of softwares: StarLogo version 2.0 (<http://education.mit.edu/starlogo/>) supplied by MIT Media Laboratory and Recursive Porous Agent Simulation Toolkit (RePast-3.0, <http://repast.sourceforge.net/>) supplied by the Argonne National Laboratory. StarLogo uses Logo, one of the simplest programming languages, and has a fixed graphical user interface. RePast is a library that uses Java, another programming language, which also has a fixed graphical user interface.

Logo is an assembly language, and StarLogo carries out processing sequentially. Java is an object-oriented language, and RePast has a faster processing speed than StarLogo. In addition, StarLogo has a number of stipulations to simplify simulations, such as parameters can only be set up to five decimal places and the simulation space is also fixed as 51×51 square grids. RePast, on the other hand, has fewer such restrictions. Thus, it offers a higher degree of freedom in program settings than StarLogo. Taking simulation space as an example, in spite of the restrictions imposed by the underlying operating system's image display system, any number of grids can be set and a hexagonal grid could also be chosen rather than a square one. However, users must stipulate and set all parameters themselves. This means that they must first declare the shape of the grid and the number of grids they will use to fill the simulation space. Java is also more difficult to learn than Logo, and debugging and correcting the program is also more difficult. Thus, it is difficult to judge whether or not the results agree with the planned simulation.

In effect, these two different types of softwares are polar opposites. It is simple to start a simulation in StarLogo, but producing results takes time and it is difficult to carry out more complex simulations. In RePast it is difficult to compose the program and judge whether or not the planned study has actually been achieved, but the

simulation itself takes only a short time to complete and there are lesser restrictions in the construction of a simulation model.

2.2. Concept for Modeling

We applied the basic virus–host interaction mathematical model to the agent-based simulation system with slight modifications. The mathematical model was used to describe the dynamics of HIV (Ho et al., 1995), HBV (Nowak et al., 1996), and HCV (Neumann et al., 1998) and the only agents involved were host cells and viruses, without the inclusion of immune cells. The effects of the immune system are expressed by varying parameters such as lifespan of host cells and viruses.

Fig. 1a illustrates the study concept. Viruses have the ability to infect healthy host cells (uninfected cells) and the infected cells produce new viruses. Both cells and viruses have definite lifespans, and the lifespan of infected cells is usually shorter than that of uninfected cells. Uninfected cells automatically regenerate within the space, whereas infected cells only arise due to infection of uninfected cells. Viruses also lack the ability to regenerate themselves and are only produced from infected cells.

2.3. Parameter Settings

In the present study, as the StarLogo settings are circumscribed, we limited the simulation space to 51 × 51 square grids. However, we made an exception here while investigating the effects of size of space on the simulation results. The numbers of viruses, uninfected cells, and infected cells could only be set before the start of the simulation. As described in the later, our simulation ran in cycles, with 1 cycle defined as 1 tic.

In mathematical simulation models, the death rate is required as a parameter. However, in our program we set lifespans for viruses and uninfected cells. These lifespans were not uniform, but were set to have a deviation of about 10%. The lifespan of cells was shortened by infection with ratio decided beforehand.

The infection ratio was meaningful only when an infected cell and a virus coincidentally occupied the same grid, and this was used to calculate the probability of the infection occurring in that situation. The virus production rate was set as the number of viruses produced by an infected cell during 1 tic. Infected cells could be set as a parameter indicating the latent period between the time of virus infection and the time of virus replication.

In order to emulate the tissue repair capacity, we set uninfected cell regeneration rate such that grids without any cells had a specified probability of producing uninfected cells on top of themselves. As a result, the more the cell count declined within a space the more regenerated uninfected cells were produced, whereas the number of regenerated cells declined as cell count increased.

The number of grids through which a virus could move in 1 tic was set as the speed of movement, and the direction of movement was set within a range of 90° toward the top of the simulation space. The program used a circulatory method of movement; when a virus arrived at the top of the space, it was translocated to the bottom, and moved again toward the top. Cells were fixed on the grid.

2.4. Simulation Flowchart

Fig. 1b shows a flowchart of the program. First, the simulation space was produced, after which each parameter was defined and the initial settings were made. Next the agents – viruses and uninfected and infected cells – were produced. The simulation cycle was as follows. Viruses moved to a new grid, and if an uninfected cell was present, this was infected with a probability based on the infection rate. The lifespan of the virus decreased, and viruses that had completed their lifespan and those that had caused an infection were removed from the space. Infected cells produced new viruses, the lifespans of both uninfected and infected cells decreased. Then, cells that had completed their lifespan were eliminated and a new cycle began. The program was set such that the simulation ended after this cycle had repeated 1000 times. This meant that one simulation was complete after 1000 tics.

2.5. Data Collection

The RePast model was programmed such that data for each tic was saved automatically as a text file at the end of the simulation. This text file could be opened by a database software. The StarLogo model was programmed to stop the simulation and collect data after every 50 tics.

2.6. Mathematical Model

In order to compare the results of this agent-based simulation, we used a viral infection mathematical model, which we improved as follows.

$$\frac{dT}{dt} = s[2601 - (T + I)] - dT - bVT \tag{1}$$

$$\frac{dI}{dt} = bVT - dI \tag{2}$$

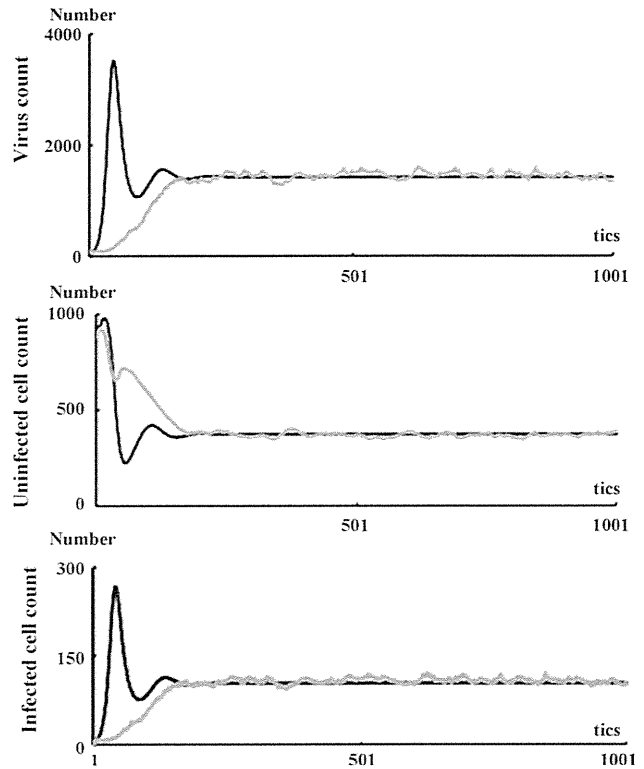


Fig. 3. Comparison of results of agent-based simulation and mathematical simulation. Both sets of results were consistent for the equilibrium phase, but differed in the shift in transition phase. Black line: mathematical model; grey line: results of simulation in RePast. Parameter values were set as follows: initial virus count, 100; uninfected cell count, 880; infected cell count, 0; virus speed of movement, 5 grids/tic; infection rate, 10%; uninfected cell regeneration rate, 1%; latent period, 3 tics; virus reproduction rate, 5/cells/tic; virus lifespan, 10 tics; uninfected cell lifespan, 50 tics; and cell lifespan-shortening ratio as a result of infection, 69%.

$$\frac{dV}{dt} = pI - cV \tag{3}$$

where, T is the uninfected cell count, I is the infected cell count, and V is the virus count. Uninfected cells are supplied to the space with a probability $s[2601 - (T+I)]$, as the number of grids in this agent-based simulation model was 2601 (51 × 51). The death rate of uninfected cells is d , the death rate of infected cells is δ , and the death rate of viruses is c . The infection rate is indicated by β . Viruses are released from infected cells at a probability p .

2.7. Statistical Analysis

Statistical analyses were performed by statistical tests using the program StatView 5.0 (SAS Institute Inc.). All tests of significance were two-tailed, with p values of <0.05 considered to be significant.

3. Results

3.1. Reproducibility of Chronic Viral Infection Disease Models Using Agent-based Simulation Methods

We constructed the chronic viral infection model with StarLogo library. Fig. 1c shows the simulation screen, and Fig. 1e shows one sample result. Immediately after the start of the simulation, the virus count temporarily dropped in accordance with the onset of an infection. Subsequently, the virus count started to increase with an increase in the infected cells and a decrease in the uninfected cells. After a certain number of tics (around 300 in this example), although the virus count, infected cell count, and uninfected cell count had some fluctuation, an equilibrium state was reached. We use the following descriptive terms in this paper: the transient phase is the period during which virus growth peaks, and the equilibrium phase is the period during which an equilibrium state is

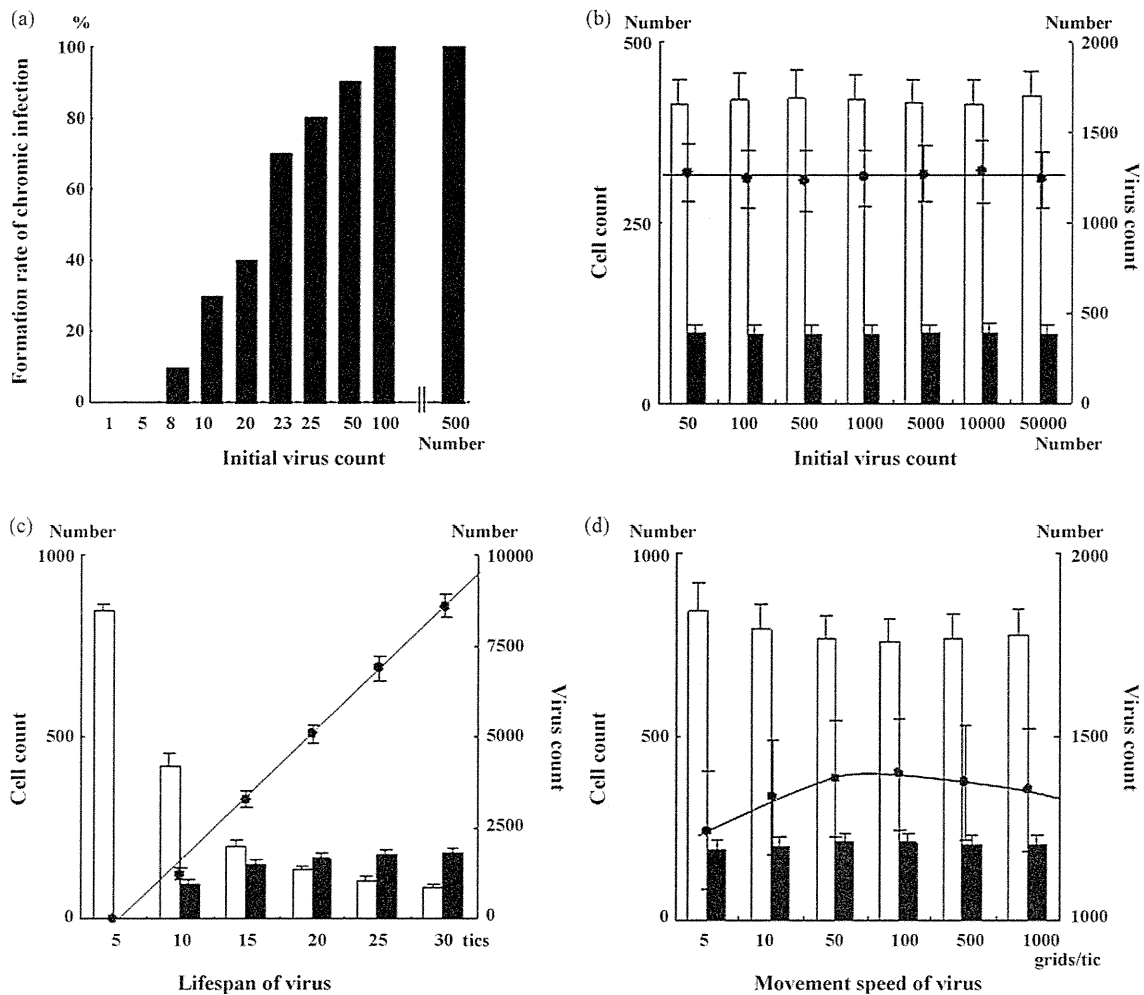


Fig. 4. Effects of changes in viral parameters. (a) The higher the initial virus count, the greater is the increase in the rate of formation of chronic infection, but (b) there was no effect on the conditions in the equilibrium phase. (c) Extending the virus lifespan increased the virus count. (d) Increasing the speed of virus movement to 100 grids/tic increased the virus count, but increasing it to 500 grids/tic had the opposite effect, with a slight declining trend. (a) Black bars: number of infections produced; (b–d) black circles: virus count; line: virus count approximation curve; white bars: uninfected cell count; black bars: infected cell count.

established. When the simulation was performed multiple times, the features described above were maintained, and the average values for virus, infected cell, and uninfected cell counts during the equilibrium state were all consistent.

Fig. 1d shows the simulation screen of the RePast. When we attempted setting all the initial parameters to the same values as those in the StarLogo, the results were not consistent. When we recalculated the parameters from the simulation results, in RePast, the parameters were largely maintained at the levels of the settings, but in StarLogo, the lifespans of both cell types became shorter than the settings while the simulation was in progress. We made the results of both simulations consistent by using the same parameters during the actual simulation (Fig. 2a and b).

3.2. Comparison Between Agent-based Simulation Models and Mathematical Simulation Model

We investigated whether the results of a chronic viral infection disease model produced by RePast would be consistent with the results of a mathematical model. For the mathematical model, we carried out an approximate integration using a four-dimensional Runge–Kutta method to ensure that the uninfected cell count and infected cell count would be in the same class. Parameters were always fixed as constant between simulations. The simulation results were consistent for the equilibrium

phase, but transitions in virus count during the transient phase varied, with a shift to equilibrium state following two overshoots in the mathematical model, but a monotonic increase following a logistic curve in the agent-based model (Fig. 3). In the mathematical model, when the equilibrium condition was calculated with $dT/dt = dI/dt = dV/dt = 0$, the equilibrium-phase virus count, uninfected cell count, and infected cell count were very similar to those of the agent-based model (virus count: mathematical model 371.8/space, agent-based model 371.1 ± 32.4 /space [average \pm SD]; uninfected cell count: mathematical model 1605/space, agent-based model 1454 ± 194 /space; infected cell count: mathematical model 115.9/space, agent-based model 108.3 ± 14.2 /space).

3.3. Usability of the Models; Effect of Changing Parameters

We investigated the changes in the equilibrium phase brought about by changing each parameter. All the investigations below were carried out by using RePast, and we used the average values from ten simulations.

3.4. Viral Parameters

The lower the virus counts at the beginning of the simulation, the lower the probability of a chronic infection (Fig. 4a). However, the initial virus count did not have any effect on the equilibrium

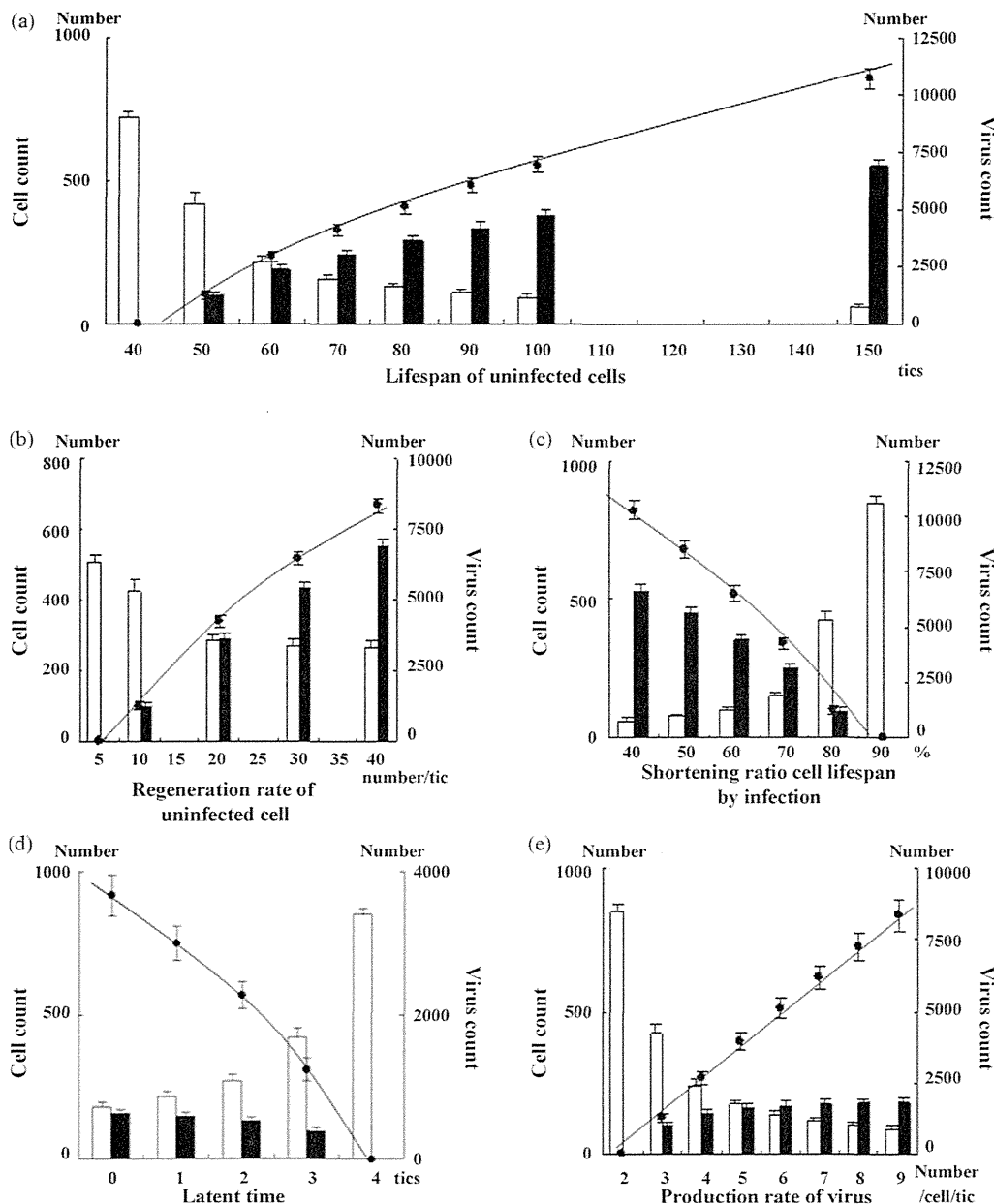


Fig. 5. Effects of changes in cell parameters. (a) Extending the uninfected cell lifespan and (b) increasing the uninfected cell regeneration rate increased the virus count. (c) Raising the lifespan-shortening ratio as a result of infection shortened the lifespan of infected cells, thereby decreasing the virus count. (d) Extending the latent period shortened the period of virus production from infected cells, thereby decreasing the virus count. (e) Increasing the virus production count resulted in a linear increase in equilibrium-phase virus count. Black circles: virus count; line: virus count approximation curve; white bars: uninfected cell count; black bars: infected cell count.

phase itself (Fig. 4b). Extending the lifespan of viruses resulted in a linear increase in equilibrium-phase virus count (Fig. 4c). Although the infected cell count increased, the rate of increase gradually declined. Changing the speed of viral movement resulted in the equilibrium-phase virus count to eventually decline after 100 grids/tic was reached, allowing movement over an area twice the size of the simulation space (Fig. 4d).

3.5. Uninfected Cell Parameters

Extending the lifespan of uninfected cells led to an increased virus count during the equilibrium phase (Fig. 5a). Increasing the uninfected cell regeneration rate also contributed to increased equilibrium-phase virus count (Fig. 5b). In both the cases, the

increases in virus count and infected cell count were not linear, but showed a tendency for the rate of increase to decline gradually.

3.6. Infected Cell Parameters

We carried out an investigation of the effects of variation in the lifespan-shortening ratio on the virus count on the assumption that cell lifespan is shortened by infection. When this ratio was increased, the virus count decreased (Fig. 5c). An extended latent period was also related to a decreased virus count (Fig. 5d). However, the virus production from infected cells led to a linear increase in the virus count (Fig. 5e).

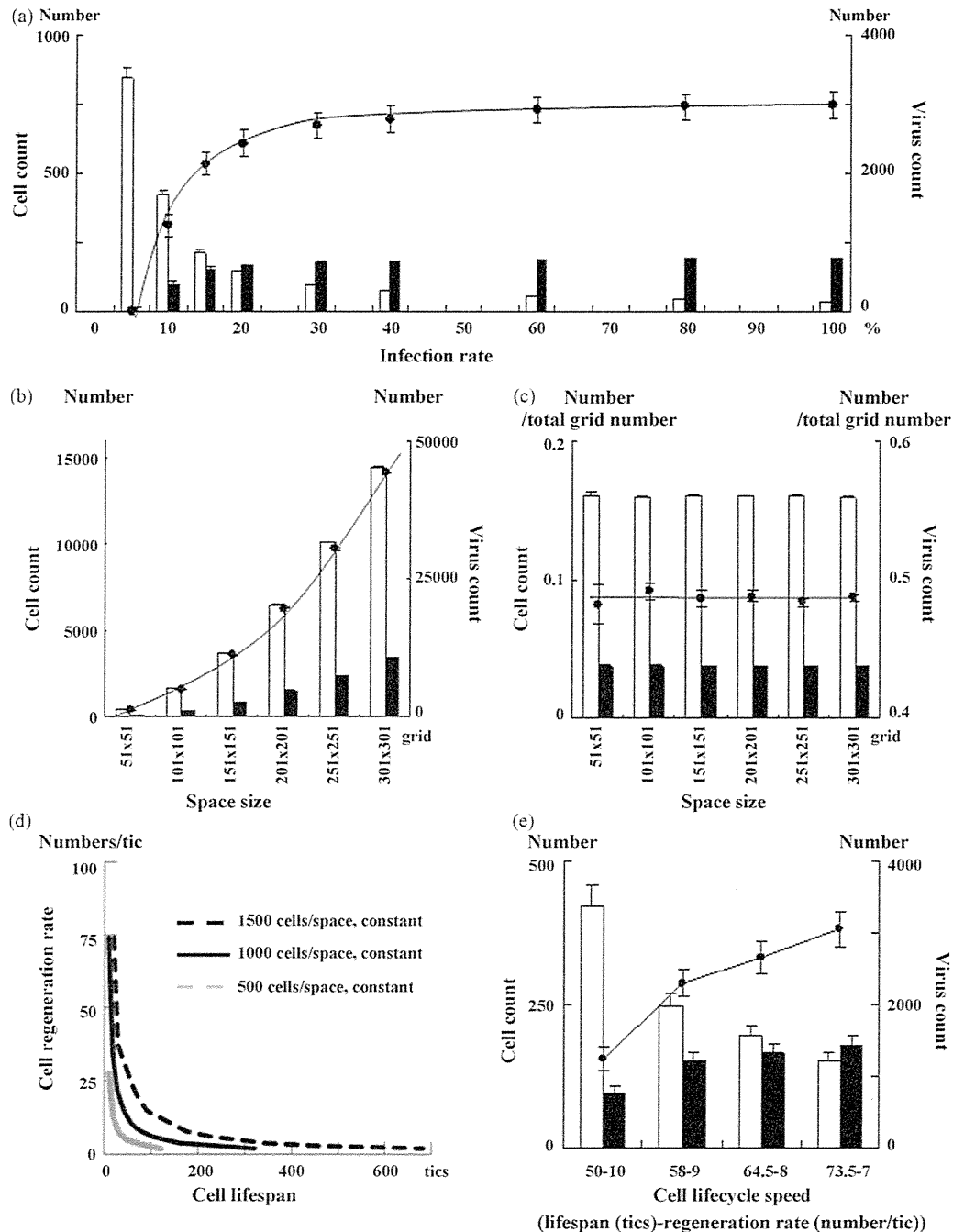


Fig. 6. (a) Increasing the infection rate increased the virus count in equilibrium periods, but the virus count did not change at infection rates of 30% or more. (b) The size of the simulation space increased not only virus count but also the cell count; however, (c) when virus and cell counts were divided by the total number of grids in the space, they were constant for all space sizes. (d) Changing the lifespan and regeneration rate of uninfected cells in opposite directions at the same time makes it possible to change only the cell cycle speed without altering the uninfected cell count. (e) When the cell cycle speed was reduced, the virus count increased toward the right of the graph. This may be because the effect of extending the lifespan of cells exceeds that of reducing their regeneration rate. (a–c and e) Black circles: virus count; line: virus count approximation curve; white bars: uninfected cell count; black bars: infected cell count.

3.7. Infection Rate and Space Size

Increasing the infection rate caused an increase in the virus count, but the change was minimal at an infection rate of 30% or more. The same results were seen for infected cell count, but a decrease in uninfected cell count resulted in a tendency for the infection rate to decrease by up to 60% (Fig. 6a).

The larger the space, higher the increase in both virus and cell counts (Fig. 6b). This increase was proportional to space size, how-

ever, when virus and cell counts were divided by the total number of grids in the space they were all constant (Fig. 6c).

3.8. Cell Cycle Speeds

Running a simulation with the initial virus count set to zero enables only the equilibrium condition for uninfected cells to be simulated. Changing the lifespan and regeneration rate of uninfected cells in opposite directions at the same time makes it possible

to change the cell cycle speed without altering the uninfected cell count (Fig. 6d). We used this technique to investigate how changing the cell cycle speed affected the equilibrium phase. Fig. 6e shows the results. Cell lifespan increases while the cell cycle speed declines. The equilibrium virus count increased in accordance with slower cell cycle speeds.

4. Discussion

In this study, we investigated the models using two agent-based simulation methods to program a simple virus–host chronic infection model. The same model written in two different programming language systems displayed the same results. The transient phase was unlike that seen in a mathematical simulation with no overshoot in virus count, but rather a smooth transition to the equilibrium phase. The virus count at the start of the simulation only had effect on the rate of infection development. Increases in virus lifespan, uninfected cell lifespan, uninfected cell regeneration rate, virus production count from infected cells, and infection rate all led to increased equilibrium-phase virus count. Rises in the infected cell lifespan-shortening ratio, latent period, and cell cycle speed decreased the equilibrium-phase virus count. The size of the space itself had no innate effect on the equilibrium phase, but a speed of movement of the virus that was twice the size of the space produced the maximum virus count.

Reproducibility is the basis for all scientific study, but there are many problems to prove it in computer simulations, such as programming bugs. As agent-based simulation deals with numerous agents individually, it requires vast amounts of calculations. Accumulation of very small change of values leads to large differences of results. In this study, we investigated two programs based on two programming languages to confirm the reproducibility of our simulation results in different programming languages. The results of two simulations were consistent, but in StarLogo, the lifespan parameters had a tendency to be lower than when they were set while simulations were actually in progress. This may be because the number of digits used in calculations was different between the two programs. RePast performs calculations to at least eight decimal places. In StarLogo, the library settings only enable settings to be made up to five decimal places. It is probable that these small differences accumulate during repeated calculations and are reflected in the simulation. Ultimately, we confirmed that the differences in results obtained by using different libraries and programming languages were not innate and by making the parameters consistent during simulation, consistent results were obtained.

Mathematical models using formulae for HIV therapy was published in 1994, the method has since been applied to HBV and HCV (Ho et al., 1995; Nowak et al., 1996; Neumann et al., 1998), and they were thought to be good reflections of the reality. In the mathematical model, viruses and cells are conceived as individuals in the concept itself, but both of them are perceived *en masse* when calculations are performed. However a feature of the agent-based simulation is that it deals with individual viruses and cells as separate agents. By moving each agent individually, it probes the factors influencing overall shifts from the micro viewpoint. When the space is viewed as a whole, it is possible to watch on the screen the collective movement of groups of agents. Recently, models that provide a visual representation of Epstein-Barr virus and HIV infection have been reported, both of which are useful for an instinctive and intuitive understanding (Duca et al., 2007; Shapiro et al., 2008; Castiglione et al., 2007).

In agent-based simulation model, virus count transit smoothly to the equilibrium phase. On the other hand, virus counts overshoot during transient phase in mathematical model. We think this difference is derived from technicality of different model-

ing. The difference in concepts between mathematical models and agent-based models is the space. The mathematical model has no space in concept, but agents move across the space in the agent-based model. In agent-based models, the densities of virus and cells change overtime especially in the transition phase because of the limited space. These changes of the densities of virus and cells lead to the dynamic change of the encounter rate of viruses and cells. The mathematical model does not make such concept of the density; the encounter rate is constant. This may be the reason for the difference between two models in the transition phase. Since no overshoot of virus counts in transient phase had been reported from *in vivo* studies of hepatitis C virus and simian immunodeficiency virus (Dahari et al., 2005; Nowak et al., 1997), agent-based model correlates with actual biology *in vivo* at least for these viruses. The increase of initial virus count at the start of simulation correlates with higher encounter rate of viruses and cells which make the linear increasing of infection forming rate. Mathematical model can only express the infection formation rate as “infected or not”.

The importance of viral passing speed in the agent-based model is also explained by the “space”. Although the virus actually moves through the blood stream in our body and virus could not decide their moving speeds by themselves, there is most appropriate speed for virus to meet the cells on the simulation space by the highest probability. The effect of cell cycle speed should be mentioned by another affection of the space. A fast cell cycle speed means that the lifespan of uninfected cells is short. Then fast cell cycle speed leads to the short lifespan of infected cells. A higher regeneration rate for uninfected cells results in a higher rate of infection among uninfected cells by viruses, but in situations where viruses and cells are dispersed around the space this is ineffective in increasing the infection rate, as the latter depends on the probability that they will encounter one another. As a result, the infected cell count decreases during the equilibrium phase, as does the virus count.

In this study, we confirmed the reproducibility and usability of agent-based models in expressing the interaction between viruses and cells. A feature of this simulation system is that it uses the concept of space as actual space, which means that the existence of the space becomes an additional controlling factor on the simulation results. This is a concept that is absent from mathematical models. The reality is that we have a spatial existence, and an advantage of the agent-based simulation system is the fact that it accounts for the space. Another feature of the simulation system is that it enables the condition to be perceived in visual terms, making it easy to understand. However it may be affected by computer performance and by the limitations of programming languages or the program itself, this system may offer a powerful tool for the future analysis of real virus–host interaction disease.

Conflict of interest

No conflicts of interest exist for all authors.

References

- Castiglione, F., Pappalardo, F., Bernaschi, M., Motta, S., 2007. Optimization of HAART with genetic algorithms and agent-based models of HIV infection. *Bioinformatics* 23, 3350–3355, doi:10.1093/bioinformatics/btm408.
- Dahari, H., Major, M., Zhang, X., Mihalik, K., Rice, C.M., Perelson, A.S., Feinstone, S.M., Neumann, A.U., 2005. Mathematical modeling of primary hepatitis c infection: noncytolytic clearance and early blockage of virion production. *Gastroenterology* 128, 1056–1066, doi:10.1053/j.gastro.2005.01.049.
- Duca, K.A., Shapiro, M., Delgado-Eckert, E., Hadinoto, V., Jarrah, A.S., Laubenbacher, R., Lee, K., Luzuriaga, K., Polys, N.F., Thorley-Lawson, D.A., 2007. A virtual look at Epstein-Barr virus infection: biological interpretations. *PLoS Pathog.* 3, 1388–1400, doi:10.1371/journal.ppat.0030137.
- Gilbert, N., Bankes, S., 2002. Platforms and methods for agent-based modelling. *Proc. Natl. Acad. Sci. U.S.A.* 99 (Suppl. 3), 7197–7198.

- Ho, D.D., Neumann, A.U., Perelson, A.S., Chen, W., Leonard, J.M., Markowitz, M., 1995. Rapid turnover of plasma virions and CD4 lymphocytes in HIV-1 infection. *Nature* 373, 123–126, doi:10.1038/373123a0.
- Naniche, D., 2009. Human immunology of measles virus infection. *Curr. Top. Microbiol. Immunol.* 330, 151–171.
- Neumann, A.U., Lam, N.P., Dahari, H., Gretch, D.R., Wiley, T.E., Layden, T.J., Perelson, A.S., 1998. Hepatitis C viral dynamics in vivo and the antiviral efficacy of interferon-alpha therapy. *Science* 282, 103–107, doi:10.1126/science.282.5386.103.
- Nowak, M.A., Bonhoeffer, S., Hill, A.M., Boehme, R., Thomas, H.C., McDade, H., 1996. Viral dynamics in hepatitis B virus infection. *Proc. Natl. Acad. Sci. U.S.A.* 93, 4398–4402.
- Nowak, M.A., Lloyd, A.L., Vasquez, G.M., Wiltout, T.A., Wahl, L.M., Biscoberger, N., Williams, J., Kinter, A., Fauci, A.S., Hirsch, V.M., Lifson, J.D., 1997. Viral dynamics of primary viremia and antiretroviral therapy in simian immunodeficiency virus infection. *J. Virol.* 71, 7518–7525.
- Shapiro, M., Duca, K.A., Lee, K., Delgado-Eckert, E., Hawkins, J., Jarrah, A.S., Laubenbacher, R., Polys, N.F., Hadinoto, V., Thorley-Lawson, D.A., 2008. A virtual look at Epstein-Barr virus infection: simulation mechanism. *J. Theor. Biol.* 252, 633–648, doi:10.1016/j.jtbi.2008.01.032.
- See, H., Wark, P., 2008. Innate immune response to viral infection of the lungs. *Paediatr. Respir. Rev.* 9, 243–250, doi:10.1016/j.prrv.2008.04.001.